

Crystallization Behavior and UV-Protection Property of PET-ZnO Nanocomposites Prepared by *In Situ* Polymerization

Junqing He, Wei Shao, Ling Zhang, Chao Deng, Chunzhong Li

Key Laboratory for Ultrafine Materials of Ministry of Education, School of Materials Science and Engineering, East China University of Science and Technology, Shanghai 200237, People's Republic of China

Received 18 June 2008; accepted 5 April 2009

DOI 10.1002/app.30614

Published online 18 June 2009 in Wiley InterScience (www.interscience.wiley.com).

ABSTRACT: The aim of this study was to investigate the crystallization behavior and UV-protection property of polyethylene terephthalate (PET)-ZnO nanocomposites. PET-ZnO nanocomposites containing 0.5–3.0 wt % of ZnO were successfully synthesized by *in situ* polymerization. The Fourier transformed infrared (FTIR) spectroscopy indicated the silane coupling agent was anchored onto the surface of ZnO. Scanning electron microscope (SEM) images showed ZnO particles were dispersed homogeneously in PET matrix with amount of 0.5–1.0 wt %. Differential scanning calorimetry (DSC) results exhibited that the incorporation of ZnO into PET resulted in increase of the melting transition temperature (T_m) and crystallization temperature (T_c) of PET-ZnO nanocomposites. The crystallization

behavior of PET and PET-ZnO nanocomposites was strongly affected by cooling rate. ZnO nanoparticles can act as an efficient nucleating agent to facilitate PET crystallization. UV-vis spectrophotometry showed that UV-ray transmittance of PET-ZnO nanocomposites decreased remarkably and reached the minimum value of 14.3% with 1.5 wt % of ZnO, compared with pure PET whose UV-ray transmittance was 84.5%. PET-ZnO nanocomposites exhibited better UV-protection property than pure PET, especially in the range of UVA. © 2009 Wiley Periodicals, Inc. *J Appl Polym Sci* 114: 1303–1311, 2009

Key words: crystallization; modification; nanocomposites; *in situ* polymerization; UV-protection property

INTRODUCTION

It is well known that ultraviolet radiation can be classified into UVA (315–400 nm), UVB (280–315 nm), and UVC (200–280 nm) regions. UVA and UVB are the main causes of the damage to human health,^{1,2} which may cause erythema, certain skin cancers, keratitis, and cataracts.^{3–6} The common method to protect skin from ultraviolet radiation with clothing, such as cotton, silk, wool, and synthetic fabrics, is not very effective because of the high UV-ray transmittance of the fabrics.⁷ Thus, it is

essential to prepare functional polyester fibers with high UV-protection property in the range of UVA and UVB, which can prevent the injuries to human bodies from UV radiation.^{8,9} There are usually two methods to improve the UV-protection property of textile fibers, surface coating, and adding UV-protection fillers into fibers. The latter method is more commonly used because it can endow textiles with higher UV-protection property, longer lifetime of UV-protection, and less influence on appearance of textiles.^{10,11} The UV-protection agents can be divided into two kinds: organic absorbers and inorganic blockers.^{12–15} Inorganic UV blockers are used widely because of their higher chemical stability, thermal stability, nontoxicity, and nonirritant compared with organic absorbers. ZnO is a wide band gap semiconductor with a band gap of 3.37 eV and an excitation banding energy of 60 meV,¹⁶ which is much larger than other wide band gap semiconductors. Because of the high UV-protection property in the range of wavelength 240–380 nm and low refractive index ($n = 1.9$), ZnO is considered as an ideal UV blocker and usually added into cosmetics for ultraviolet protection.^{17–20}

Polyethylene terephthalate (PET) absorbs UV radiation at wavelengths below 300 nm. To achieve and improve good skin protection, ZnO nanoparticles

Correspondence to: C. Li (czli@ecust.edu.cn).

Contract grant sponsor: National Natural Science Foundation of China; contract grant numbers: 20706015, 50703009.

Contract grant sponsor: Shanghai Rising-Star Program; contract grant numbers: 06QA14013, 07QA14014.

Contract grant sponsor: Major Basic Research Project of Shanghai; contract grant number: 07DJ14001.

Contract grant sponsor: Special Projects for Key Laboratories in Shanghai; contract grant numbers: 07DZ22016, 06DZ22008.

Contract grant sponsor: Special Projects for Nanotechnology of Shanghai; contract grant numbers: 0752nm010, 0652nm034.

can be applied during polymerization process of PET.^{21,22} However, it is very difficult to make these nanoparticles dispersed homogeneously in polymer matrix.²³ Nanoscaled ZnO possesses large specific surface area and high surface energy, which may cause agglomeration of particles in PET matrix and decline in performance of the nanocomposites.^{24–27} To prevent the formation of agglomerated nanoparticles, surface modification of ZnO is necessary.^{28–33}

In our previous work, we reported the preparation of PET/ATO nanocomposites by *in situ* polymerization. The results obtained indicated that ATO nanoparticles were dispersed homogeneously in PET matrix by adding silane coupling agent. The presence of ATO enhanced the crystallinity of PET by acting as a heterogeneous nucleation agent, and improved the conductivity of PET obviously. The electrical resistivity of PET/ATO fibers reached $4.9 \times 10^8 \Omega \text{ cm}$ when ATO content was 1.0 wt %.^{34–36} In this study, UV-protection PET-ZnO nanocomposites were successfully synthesized. ZnO nanoparticles were treated with silane coupling agent to introduce organic functional groups onto the surface of ZnO, which improved their compatibility, and led to better dispersion of ZnO nanoparticles in PET matrix. The effects of ZnO on morphology, crystallization behavior, and UV-protection property of PET-ZnO nanocomposites were investigated.

EXPERIMENTAL

Materials

The organic-inorganic nanocomposites were prepared by *in situ* polymerization with terephthalic acid, ethylene glycol, ZnO modified by silane coupling agent, cobalt acetate, antimony[III] oxide, and trimethyl phosphate. Terephthalic acid was purchased from Institute of Jinshan petrochemical. ZnO nanoparticles were synthesized using zinc chloride and oxalic acid by liquid phase precipitation method in our laboratory. Zinc chloride, oxalic acid, and ethylene glycol were purchased from Shanghai Lingfeng Chemical Agent Company (China). Silane coupling agent (gamma-aminopropyltriethoxysilane) used to modify ZnO nanoparticles was purchased from Nanjing Shuguang Chemical Factory. Cobalt acetate was purchased from Shanghai Hengxin Chemical Agent Company (China). Antimony[III] oxide and trimethyl phosphate were purchased from Shanghai Chemical Agent Company of medicament in China.

Synthesis of ZnO nanoparticles

ZnO nanoparticles used in this study were synthesized by liquid phase precipitation method. Aqueous

solutions of ZnCl₂ and oxalic acid were added into a flask under vigorous stirring. The molar ratio of Zn²⁺ to oxalic acid was about 1 : 2. After stirring for 2 h, the white precipitates of zinc oxalate dehydrate was obtained. The precipitates were then filtered, washed with distilled water and alcohol for several times, dried under a vacuum at 80°C for 24 h and finally calcined at 350°C for 2 h to achieve the zinc oxide nanoparticles.

Surface modification and dispersion of ZnO nanoparticles

To improve the compatibility of polyester matrix and ZnO powders, surface modification of ZnO nanoparticles is necessary before the synthesis of PET-ZnO composites. A measured amount of ZnO nanoparticles and deionized water were mixed in the stainless steel pot with zirconia balls under continuous stirring. A totla of 1.0 wt % silane coupling agent (gamma-aminopropyltriethoxysilane) was added into the mixture and the mixed solution was kept stirring for 2 h. The modified ZnO particles were dried in the oven and then transferred to a wide-mouthed plastic bottle with 100 mL ethylene glycol for further 48 h dispersion. The slurry was filtered for the preparation of PET-ZnO nanocomposites.

Preparation of PET-ZnO nanocomposites

In a typical procedure for the preparation of nanocomposites containing 1.0 wt % ZnO, a polymerization reactor (2 L) equipped with a condenser, a nitrogen inlet, and an agitator was charged with 403 g ZnO-EG mixture, 830 g terephthalic acid (PTA), 0.248 g antimony(III) oxide, 0.0173 g cobalt acetate, and 14 μL TMP. The reaction mixture was stirred for 10 min at atmospheric pressure and then heated to 240°C under the pressure of 0.15 MPa. During this esterification reaction period, continuous generation of water was observed. That temperature was maintained for 10 min after there was no water generated any more. Then, the reaction mixture was heated to 250–270°C for condensation polymerization. Finally, product was cooled to room temperature, repeatedly washed with water, and dried under a vacuum at 70°C for 24 h to obtain the PET-ZnO nanocomposites.

Characterization of PET-ZnO nanocomposites

Fourier transformed infrared spectroscopy

Fourier transformed infrared (FTIR) spectra were recorded on a Magna-IR 550 Fourier infrared spectrometer (Nicolet, USA) using KBr pellets. The spectra were collected from 4000 to 400 cm^{-1} with a 1 m^{-1} resolution over 32 scans.

Scanning electron microscope

A JEOL JSM-5600LV scanning electron microscope (SEM) (Japan) was used to observe the fractured surface morphologies of pure PET and PET-ZnO nanocomposites. Before observation, a gold layer had to be deposited on the surface of the specimen because of the nonconductivity of PET and its composites.

Differential scanning calorimeter

The thermal behavior of PET-ZnO nanocomposites was studied by differential scanning calorimetry (DSC 2910 TA Co., USA). All DSC measurements were performed under dry nitrogen flow. The samples were rapidly heated to 300°C and kept for 5 min to remove the thermal history, and then cooled to the start temperature at a rate of 5, 10, 15, and 20°C/min, respectively to study the nonisothermal crystallization behaviors of PET-ZnO nanocomposites. The specimens were subsequently heated to 300°C at a rate of 10°C/min.

UV-vis spectrophotometry

UV-ray transmittance of pure PET and PET-ZnO nanocomposites was measured on a Cary 500 ultraviolet spectrophotometer (Varian, USA). PET and PET-ZnO nanocomposites were heated to melt and coated onto glass substrates for characterizing their UV-protection property from 200 to 800 cm⁻¹.

RESULTS AND DISCUSSION

Preparation of PET-ZnO nanocomposites

Figure 1 shows the FTIR spectra of pristine ZnO, functionalized ZnO, pure PET, and PET-1.0 wt % ZnO nanocomposite. The FTIR spectrum of functionalized ZnO gave a broad absorption band located at 3400 cm⁻¹, which attributed to $\nu(\text{OH})$ and $\nu(\text{NH}_2)$.³⁷ The peaks at 2845 cm⁻¹, 2919 cm⁻¹, and 1042 cm⁻¹ can be assigned to the symmetric methylene stretch (νCH_2), antisymmetric methylene stretch (νaCH_2), and the Si—O stretch, respectively.^{38,39} The results indicated that the silane coupling agent was anchored onto the surface of ZnO nanoparticles. In the spectrum of PET-1.0 wt % ZnO composite, the new peaks at 3341 and 1042 cm⁻¹ corresponded to $\nu(\text{NH})$ and $\nu(\text{Si—O})$ of silane coupling agent, which also proved that the silane coupling agent was anchored onto the surface of ZnO and interacted well with PET matrix.⁴⁰

Morphology of PET-ZnO nanocomposites

To examine the morphology of the materials, PET-ZnO nanocomposites with different ZnO contents were observed by SEM (Fig. 2). The results showed

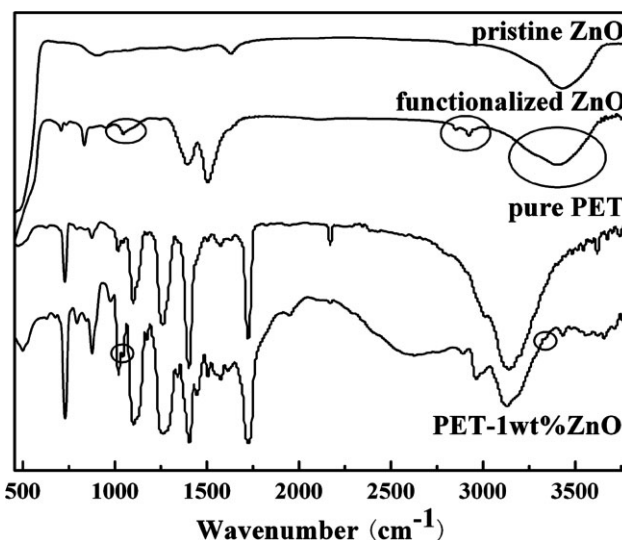


Figure 1 FTIR spectra of pristine ZnO, functionalized ZnO, pure PET, and PET-1.0 wt % ZnO nanocomposites.

that ZnO nanoparticles were homogeneously dispersed in PET matrix when the amount of ZnO was 0.5–1.0 wt %, and their average particle size was below 100 nm. With increasing the content of ZnO, the interfacial compatibility of ZnO particles and polyester matrix reduced, and the irregular aggregation of ZnO nanoparticles occurred. When the amount of ZnO reached 2.0–3.0 wt %, ZnO particles aggregated together seriously.

Crystallization behavior of PET-ZnO nanocomposites

PET is a semicrystalline polymer. Crystallization is another important feature of it. DSC was carried out to investigate the crystallization behaviors of PET and PET-ZnO nanocomposites. The samples were first heated to 300°C and kept at this temperature for 5 min, then cooled at a rate of 10°C/min to the start temperature and then heated at a rate of 10°C/min to 300°C again. Figure 3(a,b) shows DSC heating and cooling curves of pure PET and PET-ZnO nanocomposites with different ZnO contents, respectively, and Table I lists the thermal data for each of these samples.

Corresponding to the melting transition temperature (T_m), the endothermic peak of pure PET appeared at 241.74°C as shown in Figure 3(a), whereas the peaks of PET-ZnO nanocomposites moved to higher temperature compared with pure PET. The values of T_m of the nanocomposites increased with increasing ZnO content from 0.5 wt % to 2.5 wt % and decreased slightly at 3.0 wt %. However, the values of heat of fusion (H_m) of the nanocomposites changed irregularly when increasing ZnO content from 0.5 to 3.0 wt %. We speculated

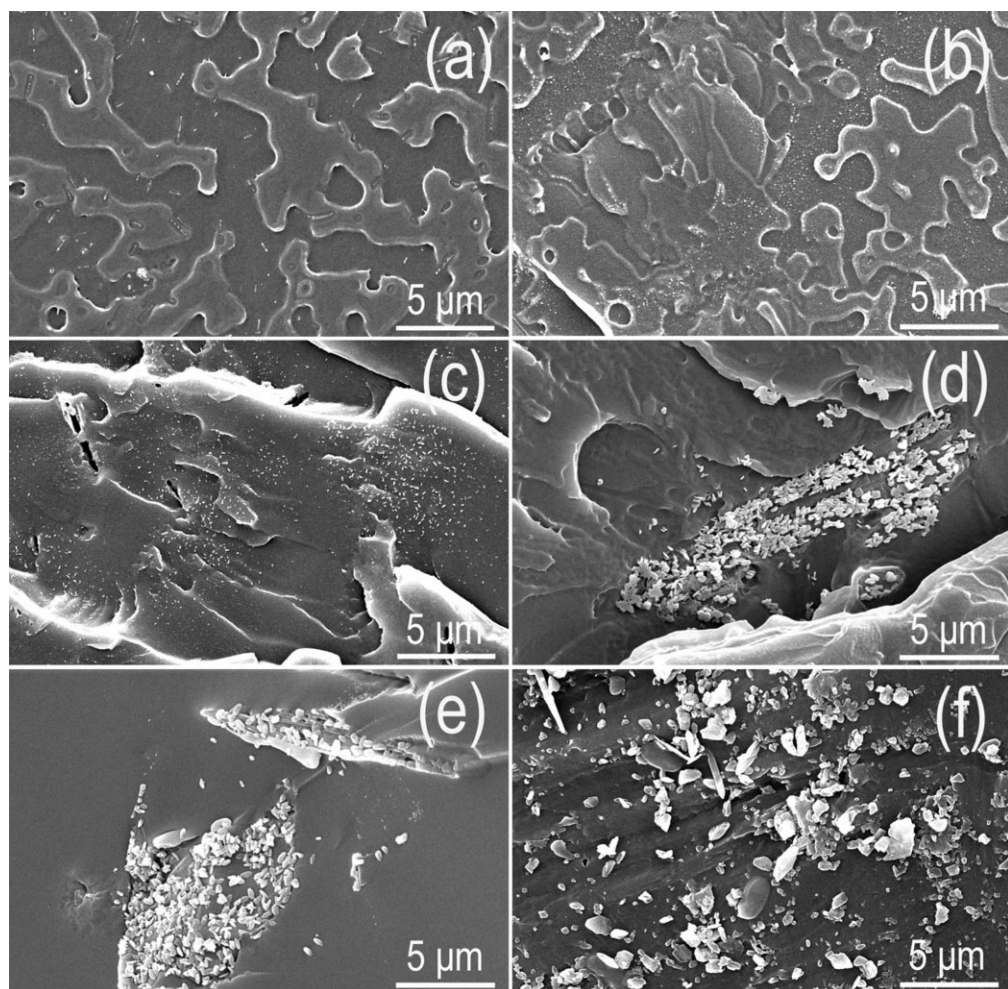


Figure 2 SEM images of PET-ZnO nanocomposites (a) PET-0.5 wt % ZnO; (b) PET-1.0 wt % ZnO; (c) PET-1.5 wt % ZnO; (d) PET-2.0 wt % ZnO; (e) PET-2.5 wt % ZnO; (f) PET-3.0 wt % ZnO.

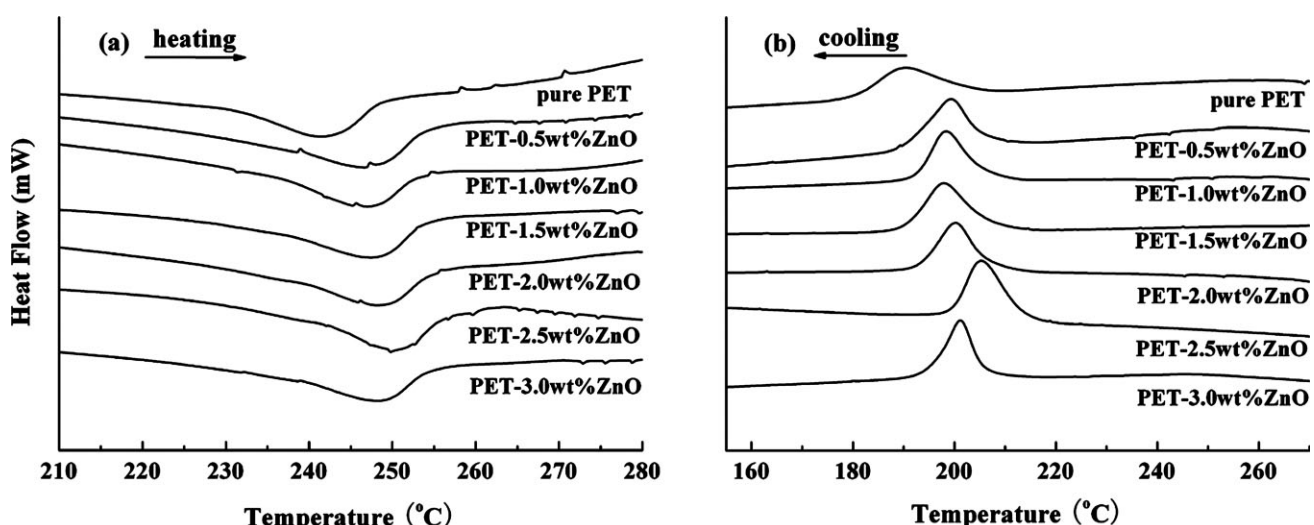


Figure 3 DSC thermograms (at heating and cooling rate of 10°C/min, respectively) for (a) heating curves and (b) cooling curves of pure PET and PET-ZnO nanocomposites with different ZnO contents.

TABLE I
Summary of DSC Heating and Cooling Data of Pure PET and PET-ZnO Nanocomposites

ZnO content (wt %)	T_c (°C)	H_c (J/g)	T_m (°C)	H_m (J/g)
0	190.29	44.2815	241.74	-32.7146
0.5	199.21	42.7118	246.87	-35.7365
1.0	198.43	42.9120	246.92	-31.5123
1.5	197.94	43.5375	247.58	-30.7195
2.0	200.28	43.0836	248.43	-32.5241
2.5	205.36	43.4996	249.80	-38.4314
3.0	201.24	41.3596	248.47	-29.8181

the possible reason was the presence of inorganic and/or polymeric components formed in the process of *in situ* polymerization of PET hid the effect of ZnO on crystallization of PET.⁴¹

From the cooling curve shown in Figure 3(b), it can be seen that the exothermic peaks of PET-ZnO nanocomposites shifted to a higher value compared with the pure PET, and the crystallization temperature increased. Therefore, ZnO nanoparticles were able to act as an efficient nucleating agent to facilitate PET crystallization, which could be further proved by the curves of relative crystallinity $X(T)$ vs. crystallization temperature in Figure 4.

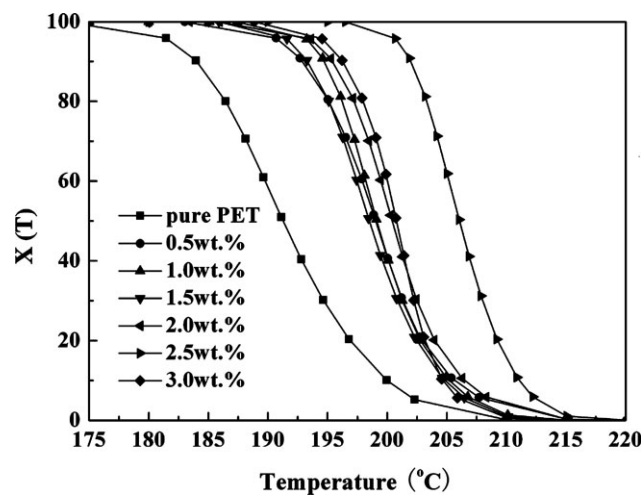


Figure 4 $X(T)$ as a function of temperature (at cooling rate of 10°C/min) for crystallization of pure PET and PET-ZnO nanocomposites with different ZnO contents.

The X_c values of PET-ZnO nanocomposites were all higher than that of pure PET and the curves of $X(T)$ vs. crystallization temperature for all samples moved toward low crystallization temperature location.

Nonisothermal crystallization behavior of PET and PET-ZnO nanocomposites with cooling rates of 5, 10, 15, and 20°C/min was investigated. Figure 5 shows

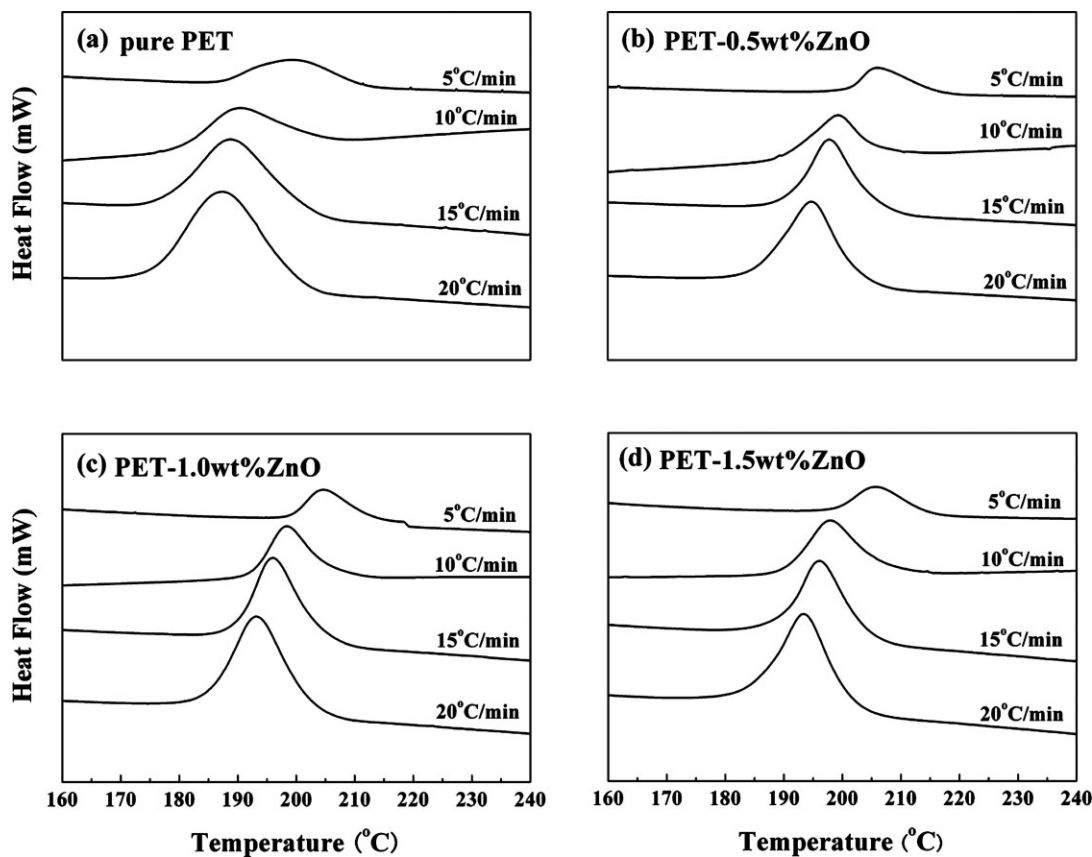


Figure 5 DSC cooling curves (at cooling rates of 5, 10, 15, and 20°C/min) of (a) pure PET and PET-ZnO nanocomposites with different ZnO contents (b) 0.5 wt %, (c) 1.0 wt %, (d) 1.5 wt %.

TABLE II
Characteristic Data of Nonisothermal Crystallization Exotherms for Pure PET and PET-ZnO Nanocomposites with Different ZnO Contents

Sample	Φ (°C/min)	T_c (°C)	ΔH_c (J/g)	X_c (%)
Pure PET	5	199.70	46.6109	33.29
	10	190.29	44.2815	31.63
	15	188.90	45.3055	32.36
	20	187.57	45.1089	32.22
PET-0.5 wt % ZnO	5	206.18	45.7592	32.85
	10	199.21	42.7118	30.66
	15	197.94	45.9125	32.96
	20	194.93	43.9887	31.58
PET-1.0 wt % ZnO	5	204.70	50.9022	36.73
	10	198.43	42.9120	30.96
	15	195.96	44.4011	32.04
	20	193.29	42.9911	31.02
PET-1.5 wt % ZnO	5	205.72	42.2344	30.63
	10	197.94	43.5375	31.57
	15	196.22	43.7355	31.72
	20	193.29	44.6674	32.39

the cooling curves of pure PET and PET-ZnO nanocomposites with different ZnO contents. It can be seen that the crystallization behavior of PET and its nanocomposites was strongly affected by cooling rate. With increasing cooling rate, the exothermic peaks shifted to a lower value, and the crystallization temperature decreased. It indicated that the crystallization rate decreased with increasing T_c . The influence of crystallization rate on crystallization

temperature was similar for pure PET and its nanocomposites with different ZnO contents, as shown in Figure 5(b-d). At the slower cooling rate, the molecular chains may have enough time to pack up in a unit cell and then their nuclei grew up more rapidly. Although the higher cooling rate made PET molecular chains be too late to arrange regularly or to form crystal nuclei so that they needed the greater supercool degree to crystallize well.⁴²

The effects of ZnO nanoparticles on the degree of crystallinity (X_c) of PET were investigated. The normalized X_c values of samples were determined, which can be calculated using the following equation:

$$X_c(\%) = \frac{\Delta H_c}{(1 - \Phi)\Delta H_m} \times 100 \quad (1)$$

where ΔH_c is the crystallization enthalpy of sample, ΔH_m is the melting enthalpy of 100% crystalline PET ($\Delta H_m = 140$ J/g), Φ is the weight fraction of ZnO in PET-ZnO nanocomposite sample (wt %). The corresponding characteristic data of nonisothermal crystallization exotherms and the DSC curves of relative crystallinity $X(T)$ as a function of crystallization temperature at different cooling rates for pure PET and PET-ZnO nanocomposites were displayed in Table II and Figure 6, respectively.

Figure 6 showed that the values of X_c decreased exponentially with rising cooling rate and the curves

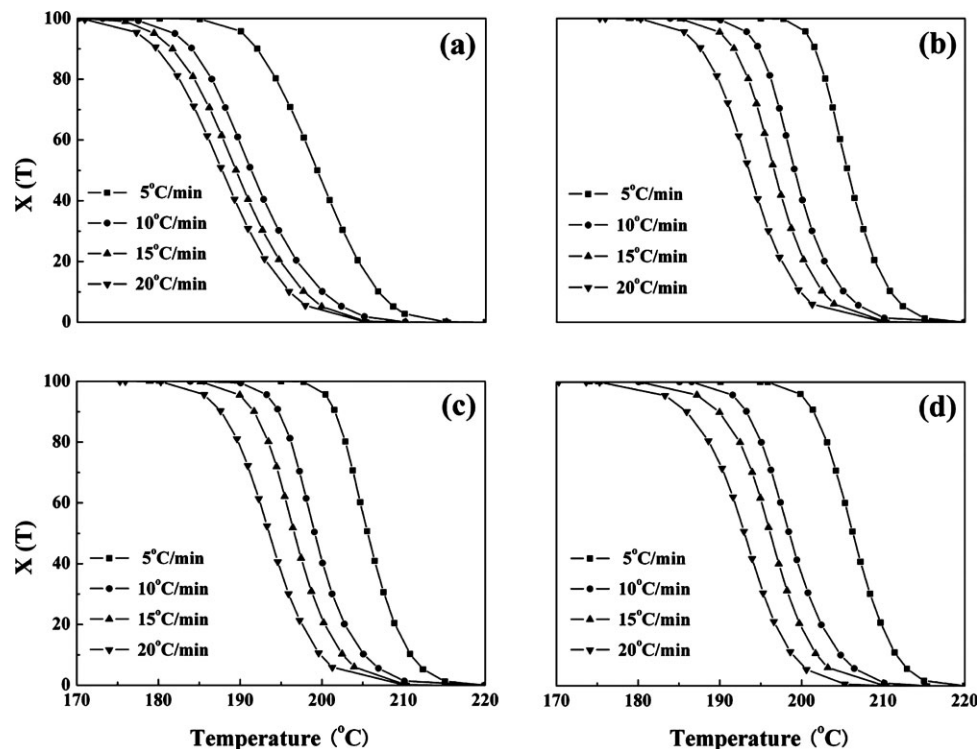


Figure 6 $X(T)$ as a function of temperature (at cooling rates of 5, 10, 15, and 20 °C/min) for crystallization of (a) pure PET and PET-ZnO nanocomposites with different ZnO contents (b) 0.5 wt %, (c) 1.0 wt %, (d) 1.5 wt %.

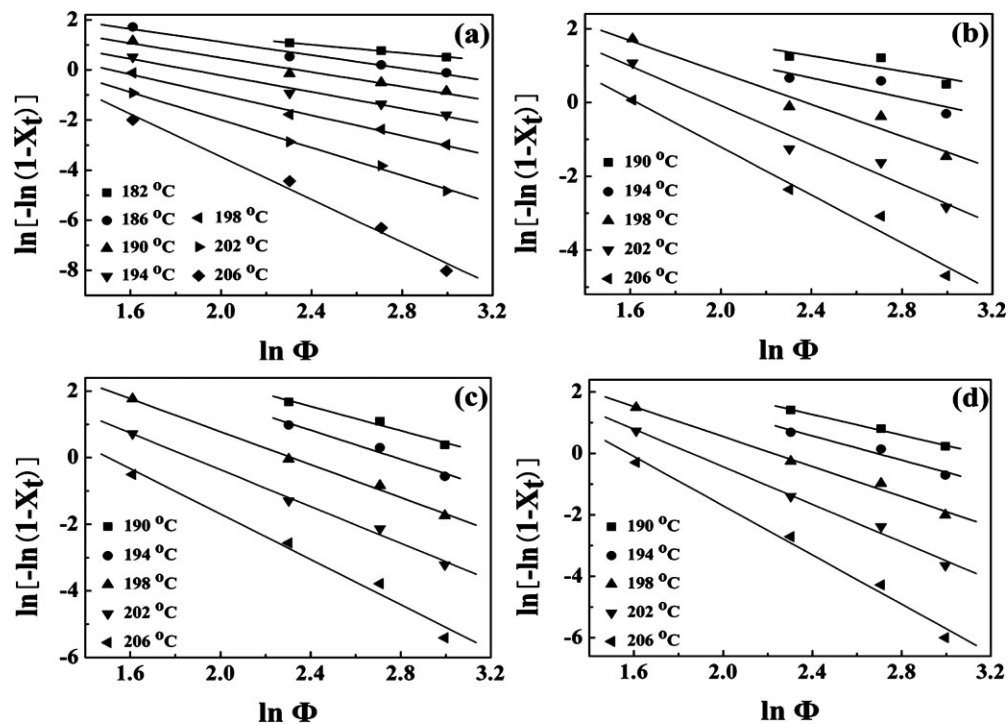


Figure 7 Ozawa plots of $\ln[-\ln(1-X_t)]$ versus $\ln \Phi$ for (a) pure PET and PET-ZnO nanocomposites with different ZnO contents (b) 0.5 wt %, (c) 1.0 wt %, (d) 1.5 wt % at different crystallization temperatures.

of $X(T)$ vs. crystallization temperature for all samples moved toward low crystallization temperature location.

The nonisothermal crystallization kinetics of PET-ZnO nanocomposite can be well approximated by Ozawa model. This model is based on the following equation:

$$\ln[-\ln(1-X_t)] = \ln K_0 - n_o \ln \Phi \quad (2)$$

where K_0 is the crystallization rate constant, X_t is the relative crystallinity, Φ is the cooling rate, and n_o is

the Ozawa coefficient depending on the crystal growth and nucleation mechanism.

By plotting $\ln[-\ln(1-X_t)]$ versus $\log \Phi$ at a given temperature, the kinetic parameters n_o and K_0 can be calculated from the slope and the intercept, respectively. It can be seen from Figure 7 and Tables III that the Ozawa treatment showed good agreement modeling the crystallization behavior of PET-ZnO nanocomposite.

According to Bian's opinion, n values relate with the number of growth points in crystal nuclei,

TABLE III
Nonisothermal Crystallization Kinetic Parameters Based on the Ozawa Method

T (°C)	Pure PET			PET-0.5 wt % ZnO		
	K_0 (min ⁻¹)	n_o	r^2	T (°C)	K_0 (min ⁻¹)	n_o
182	19.439	0.82	0.998	190	41.616	1.03
186	41.999	1.31	0.973	194	45.710	1.32
190	29.174	1.44	0.974	198	168.210	2.16
194	21.847	1.65	0.981	202	192.690	2.67
198	21.852	2.04	0.991	206	199.324	3.25
202	34.544	2.77	0.997			
206	159.030	4.27	0.987			
PET-1.0 wt % ZnO						
190	374.177	1.83	0.976	190	201.259	1.68
194	428.886	2.18	0.972	194	199.491	1.97
198	306.731	2.47	0.996	198	228.010	2.44
202	174.302	2.76	0.994	202	295.613	3.06
206	166.547	3.40	0.980	206	549.468	4.01
PET-1.5 wt % ZnO						

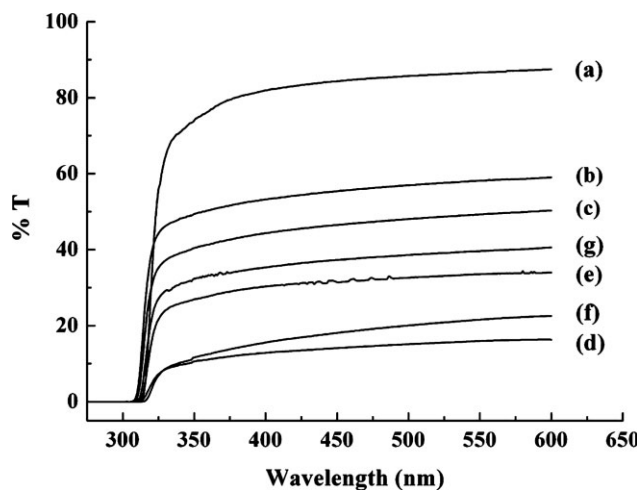


Figure 8 Spectrogram of UV-ray transmitting of (a) pure PET and PET-ZnO nanocomposites with different ZnO contents (b) 0.5 wt %; (c) 1.0 wt %; (d) 1.5 wt %; (e) 2.0 wt %; (f) 2.5 wt %; (g) 3.0 wt %.

namely, the bigger the number is, the larger the n values.⁴³ Table III showed that the obtained n_o values lay between 0.82 and 4.27 for pure PET, between 1.03 and 3.25 for PET-0.5 wt % ZnO, between 1.83 and 3.40 for PET-1.0 wt % ZnO, and between 1.68 and 4.01 for PET-1.5 wt % ZnO, with average values of 2.04, 2.09, 2.53, and 2.63, respectively. The n_o values of PET-ZnO composites were larger than that of pure PET. Therefore, the incorporation of ZnO resulted in the addition of the crystallizing growth points.

In the process of crystallization of pure PET and PET-ZnO composites, the average values of K_O , which were related to nucleation rate and growth processes, were 46.841 min⁻¹ for pure PET, 129.51 min⁻¹ for PET-0.5 wt % ZnO, 290.129 min⁻¹ for PET-1.0 wt % ZnO and 294.768 min⁻¹ for PET-1.5 wt% ZnO, respectively. It can be seen that K_O values of PET-ZnO composites were larger than that of pure PET. The incorporation of ZnO nanoparticles increased the crystallization kinetic constant K_O , suggesting that ZnO nanoparticles can act as effective nucleating agents and accelerate the crystallization of PET in the nanocomposites.³⁴

UV-protection property of PET-ZnO nanocomposites

To investigate the effect of ZnO nanoparticles on the UV-protection property of PET, UV-ray transmittance of PET and PET-ZnO nanocomposites was determined and plotted in Figure 8. It can be easily seen from this figure that PET-ZnO nanocomposites exhibited better UV-protection property than pure PET in the range of UVA (320–400 nm). The UV-ray transmittance of PET-ZnO nanocomposites

decreased remarkably with increasing ZnO contents, and reached the minimum value of 14.3% when ZnO content was 1.5 wt %, compared with pure PET whose UV-ray transmittance was 84.5%. However, the UV-ray transmittance of nanocomposites increased with increasing the ZnO content from 1.5 wt % to 3.0 wt %. This could be attributed to the agglomeration of zinc oxide nanoparticles. From Figure 8, it could be concluded that ZnO nanoparticles can improve UV-protection property of PET remarkably in the range of UVA, although some ZnO nanoparticles aggregated in PET matrix.

CONCLUSIONS

PET-ZnO nanocomposites were prepared by *in situ* polymerization. The effects of ZnO nanoparticles on the crystallization behavior and UV-protection property of PET and its nanocomposites have been comparatively investigated in detail. ZnO nanoparticles were homogeneously dispersed in PET matrix with the content of 0.5–1.0 wt %, but aggregated with increasing ZnO content. DSC results confirmed that ZnO nanoparticles enhanced the crystallization rate of PET, and led to a large increase in the crystallization temperature. The isothermal crystallization behavior of PET and PET-ZnO composites was strongly influenced by cooling rate. The crystallization temperature and the degree of crystallinity decreased with increasing cooling rate. The UV-protection property of PET was improved by adding ZnO nanoparticles. The nanocomposite gained the best UV-protection property when ZnO content was 1.5 wt %.

References

1. Mondal, S.; Hu, J. L. *J Appl Polym Sci* 2007, 103, 3370.
2. Lu, H. F.; Fei, B.; Xin, J. H.; Wang, R. H.; Li, L. *J Colloid Interf Sci* 2006, 300, 111.
3. Yang, H. Y.; Zhu, S. K.; Pan, N. *J Appl Polym Sci* 2004, 92, 3201.
4. Yamaguchi, Y.; Beer, J. Z.; Hearing, V. J. *Arch Dermatol Res* 2008, 300, S43.
5. Gallagher, R. P.; Lee, T. K. *Prog Biophys Mol Bio* 2006, 92, 119.
6. Yasuhiro, M.; Ananthaswamy, H. N. *Toxicol Appl Pharm* 2004, 195, 298.
7. Teng, C. Q.; Yu, M. H. *J Appl Polym Sci* 2003, 88, 1180.
8. Czajkowski, W.; Paluszakiewicz, J.; Stolarski, R.; Kaźmierska, M.; Grzesiak, E. *Dyes Pigments* 2006, 71, 224.
9. Tarbuk, A.; Grancaric, A. M.; Jancijev, I.; Sharma, S. *Tekstil* 2006, 55, 383.
10. Ibrahim, N. A.; Refai, R.; Youssef, M. A.; Ahmed, A. F. *J Appl Polym Sci* 2005, 97, 1024.
11. Gorenek, M.; Sluga, F. *Text Res J* 2004, 74, 469.
12. Aloui, F.; Ahajji, A.; Irmouli, Y.; George, B.; Charrier, B.; Merlin, A. *Appl Surf Sci* 2007, 253, 3737.
13. Nasu, A.; Otsubo, Y. *J Colloid Interf Sci* 2007, 310, 617.
14. El-Boury, S.; Couteau, C.; Boulannde, L.; Paparis, E.; Coiffard, M. L. *J. Int J Pharm* 2007, 340, 1.

15. Serpone, N.; Dondi, D.; Albini, A. *Inorg Chim Acta* 2007, 360, 794.
16. Vaishnavi, T. S.; Haridoss, P.; Vijayan, C. *Mater Lett* 2008, 62, 1649.
17. Hayashi, S.; Takeshita, H.; Nagao, N.; Nikaido, O.; Miwa, N. *J Photochem Photobio B* 2001, 64, 27.
18. Yadav, A.; Prasad, V.; Kathel, A. A.; Raj, S.; Yadav, D.; Sundaramoorthy, C.; Vigneshwaran, N. *Bull Mater Sci* 2006, 29, 641.
19. Vigneshwaran, N.; Kumar, S.; Kathe, A. A.; Varadarajan, P. V.; Prasad, V. *Nanotechnology* 2006, 17, 5087.
20. Katangur, P.; Patra, P. K.; Warner, S. B. *Polym Degrad Stab* 2006, 91, 2437.
21. Han, K. Q.; Yu, M. H. *J Appl Polym Sci* 2006, 100, 1588.
22. Liauw, C. M.; Childs, A.; Allen, N. S.; Edge, M.; Franklin, K. R.; Collopy, D. G. *Polym Degrad Stab* 1999, 65, 207.
23. Tang, L. Q.; Bing, Z.; Tian, Y. M.; Bala, H.; Pan, Y.; Ren, S. X.; Wang, Y.; Lv, X. T.; Li, M. G.; Wang, Z. C. *Colloid Surf A* 2007, 296, 92.
24. Althues, H.; Henle, J.; Kaskel, S. *Chem Soc Rev* 2007, 36, 1454.
25. Guo, Z. H.; Wei, S. Y.; Shedd, B.; Scaffaro, R.; Pereira, T.; Thomas, H. H. *J Mater Chem* 2007, 17, 806.
26. Tang, E.; Cheng, G. X.; Ma, X. L.; Pang, X. S.; Zhao, Q. *Appl Surf Sci* 2006, 252, 5227.
27. Hong, R. Y.; Qian, J. Z.; Cao, J. X. *Powder Technol* 2006, 163, 160.
28. Chen, G. L.; Chen, S. H.; Feng, W. R.; Chen, W. X.; Yang, S. Z. *Appl Surf Sci* 2008, 254, 3915.
29. Legrand, S.; Catheline, A.; Kind, L.; Constable, E. C.; Housecroft, C. E.; Landmann, L.; Banse, P.; Pieles, U.; Wirth-Heller, A. *N J Chem* 2008, 32, 588.
30. Goodarzi, V.; Monemian, S. A.; Maleki, F.; Angaji, M. T. *J Macromol Sci Phys* 2008, 47, 472.
31. Do Kim, K.; Min, S. S.; Choa, Y. H.; Kim, H. T. *J Ind Eng Chem* 2007, 13, 1137.
32. Tang, E.; Tian, B.; Zheng, E.; Fu, C. Y.; Cheng, G. X. *Chem Eng Commun* 2008, 195, 479.
33. Emi, U.; Takeshi, F.; Masahide, S.; Noboru, S. *Appl Surf Sci* 2007, 254, 563.
34. Chen, X. L.; Li, C. Z.; Shao, W. *Eur Polym J* 2007, 43, 3177.
35. Chen, X. L.; Li, C. Z.; Shao, W.; He, J. Q. *J Appl Polym Sci* 2007, 105, 2783.
36. Chen, X. L.; Li, C. Z.; Shao, W.; Du, H. L.; Burnell-Gray, J. S. *J Appl Polym Sci* 2007, 105, 1490.
37. Labuayai, S.; Promarak, V.; Maensiri, S. *Appl Phys A* 2009, 94, 755.
38. Turgeman, R.; Gershevitz, O.; Palchik, O.; Deutsch, M.; Ocko, B. M.; Gedanken, A.; Sukenik, C. N. *Cryst Growth Des* 2004, 4, 169.
39. El-Nahhal, I. M.; El-Ashgar, N. M. *J Organomet Chem* 2007, 692, 2861.
40. Chen, K.; Xiong, C. X.; Li, L. B.; Zhou, L.; Lei, Y. A.; Dong, L. *J Polym Compos* 2009, 30, 226.
41. Bizarria, M. T. M.; Giraldi, A. L. F. de M.; Carvalho, C. M. de; D'avila, M. A.; Mei, L. H. I. *J Appl Polym Sci* 2007, 104, 1839.
42. Ke, Y. C.; Wu, T. B.; Xia, Y. F. *Polymer* 2007, 48, 3324.
43. Bian, J.; Ye, S. R.; Feng, L. X. *J Polym Sci: Part B: Polym Phys* 2003, 41, 2135.